Block Copolymer-Mediated Synthesis of Size-Tunable Gold Nanospheres and Nanoplates

ARTICLE *in* LANGMUIR · NOVEMBER 2008

Impact Factor: 4.46 · DOI: 10.1021/la802279j · Source: PubMed

4 AUTHORS, INCLUDING:

Emilio Castro
Universidad de Sevilla
34 PUBLICATIONS **478** CITATIONS
SEE PROFILE

Pablo Taboada
University of Santiago de Compostela
147 PUBLICATIONS **2,284** CITATIONS
SEE PROFILE

Víctor Mosquera
University of Santiago de Compostela
170 PUBLICATIONS **3,079** CITATIONS
SEE PROFILE

Article

Block Copolymer-Mediated Synthesis of Size-Tunable Gold Nanospheres and Nanoplates

Sonia Goy-Lo#pez, Emilio Castro, Pablo Taboada, and Vi#ctor Mosquera

Langmuir, **2008**, 24 (22), 13186-13196• DOI: 10.1021/la802279j • Publication Date (Web): 16 October 2008

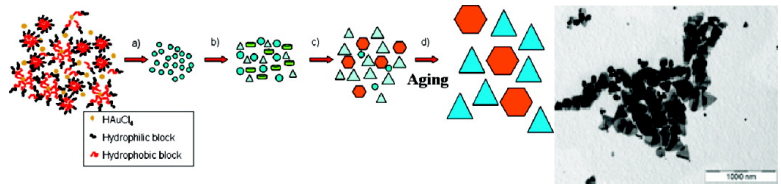

More About This Article

Additional resources and features associated with this article are available within the HTML version:

- Supporting Information
- Access to high resolution figures
- Links to articles and content related to this article
- Copyright permission to reproduce figures and/or text from this article

View the Full Text HTML

Block Copolymer-Mediated Synthesis of Size-Tunable Gold Nanospheres and Nanoplates

Sonia Goy-López, Emilio Castro, Pablo Taboada,* and Víctor Mosquera

Grupo de Física de Coloides y Polímeros; Departamento de Física de la Materia Condensada, Facultad de Física, Universidad de Santiago de Compostela, E-15782, Santiago de Compostela, Spain

Received July 16, 2008. Revised Manuscript Received September 2, 2008

We have successfully controlled the size and shape of isotropic and anisotropic gold nanocrystals through a one-step reaction by using amphiphilic polyethylene oxide−polystyrene oxide block copolymers as both reductant and stabilizing agents in water solution. Spherical or quasispherical nanoparticles were obtained at room temperature with tunable mean sizes and polydispersities depending on reaction conditions, that is, on copolymer block length, and copolymer and gold salt concentrations. By moderate increases of reaction temperature up to 65 °C, progressive formation of single-crystalline gold nanoplates in good yields takes place (up to 70%) without the necessity of additional reactants or growing solutions. These nanoplates are characterized by lateral mean sizes between 0.1−1.2 μm depending on copolymer concentration and reaction temperature, with mainly truncated or rounded triangular shapes with {111} planes as two basal surfaces. This allows us to tune the surface plasmon band of the nanoplates from ca. 850 nm to more than 1100 nm, well inside the near-infrared region (NIR), which enables the use of these type of nanostructures as a very promsing materials in applications such as optical coatings, SERS, and cancer cell hyperthermia. We proposed that the growth of these nanostructures can stem from a decrease in the reaction rate as temperature increases due to an enhanced copolymer hydrophobicity, which gives rise to a structure of interacting micelles formed from the fluid via a percolation transition (known as "soft gel") at elevated temperatures. In this way, reduction becomes slow enough to allow kinetic control of the reaction, and preferential adsorption of the copolymer molecules/micelles on certain crystallographic planes can favor the growth of certain nanocrystal facets to give the final structure. This alternative water-based system provides a more convenient and environmentally benign route to the synthesis of shape-controlled noble-metal nanocrystals in high yield because it does not involve toxic organic solvents or reagents and serves as a bridge between two frontline discipline: the block copolymeric science and anisotropic nanoparticles.

1. Introduction

Fabrication of nanostructures made of various metals has been intensively studied in the last couple of decades due to their unique properties (compared with bulk materials).[1] Among them, gold nanoparticles (Au NPs) have attracted great attention due to their fascinating size-related electronic, magnetic, and optical properties and their applications, as in surface plasmonics, surface-enhanced Raman scattering (SERS), chemical and biological sensing, photothermal therapy, and catalysis.[1,2] The properties of metal nanostructures are strongly dependent on their dimension, composition, crystallinity, shape, and construction geometry (e.g., core−shell, solid, and hollow).[3] An exquisite shape control of noble metal nanocrystals is therefore highly desirable for tailoring their properties and is also required for high performance in many applications.

The formation of a particular shape in the solution-phase synthesis of metal nanocrystals is not only addressed by the thermodynamics or physical restrictions imposed by the capping agent, which can change the order of free energies of different facets through their interactions with the metal surface altering their relative growth rates, but also nucleation and kinetics.[4] In this way, a variety of synthetic strategies for gold nanostructures based on the reduction of gold(III) precursor by various techniques in a suitable solvent has been developed in aqueous and nonhydrolitic media in the last years, the strategies including photochemistry,[5] thermochemistry[6] wet-chemistry,[7] and bio-chemistry.[8] By using these different routes, different shaped and

* To whom correspondence should be addressed. E-mail: pablo.taboada@usc.es.

(1) (a) Shipway, A. N.; Katz, E.; Willner, I. *ChemPhysChem* **2000**, *1*, 18–52. (b) Rao, C. N. R.; Cheetham, A. K. *J. Mater. Chem.* **2001**, *11*, 2887–2894. (c) Cao, Y. W.; Jin, R. C.; Mirkin, C. A. *Science* **2002**, *297*, 1536–1540. (d) Burda, C.; Chen, X. B.; Narayanan, R.; El-Sayed, M. A. *Chem. Rev.* **2005**, *105*, 1025–1102.

(2) (a) Daniel, M. C.; Astruc, D. *Chem. Rev.* **2004**, *104*, 293–346. (b) Moore, B. D.; Stevenson, L.; Watt, A.; Flitsch, S.; Turner, N. J.; Cassidy, C.; Graham, D. *Nat. Biotechnol.* **2004**, *22*, 1133. (c) Chen, J.; Wiley, B.; Li, Z.-Y.; Campbell, D.; Saeki, F.; Cang, H.; Au, L.; Lee, J.; Li, X.; Xia, Y. *Adv. Mater.* **2005**, *17*, 2255–2561. (d) Rosi, N. L.; Mirkin, C. A. *Chem. Rev.* **2005**, *105*, 1547–1542. (e) Liz-Marzán, L. M. *Langmuir* **2006**, *22*, 32–41. (f) Jana, N. R.; Pal, T. *Adv. Mater.* **2007**, *19*, 1761–1765. (g) Huang, X. H.; El-Sayed, I. H.; Qian, W.; El-Sayed, M. A. *J. Am. Chem. Soc.* **2006**, *128*, 2115–2120. (h) Hu, M.; Chen, J.; Li, Z.-Y.; Au, L.; Hartland, G. V.; Li, X.; Marquez, M.; Xia, Y. *Chem. Soc. Rev.* **2006**, *35*, 1084–1094. (i) Lewis, L. N. *Chem. Rev.* **1993**, *93*, 2693–2730. (j) Hughes, M. D.; Xu, Y.-J.; Jenkins, P.; McMorn, P.; Landon, P.; Enache, D. I.; Carley, A. F.; Attard, G. A.; Hutchings, G. J.; King, F.; Stitt, E. H.; Johnston, P.; Griffin, K.; Kiely, C. J. *Nature* **2005**, *437*, 1132–1135.

(3) (a) El-Sayed, M. A. *Acc. Chem. Res.* **2001**, *34*, 257–264. (b) Murphy, C. J.; Jana, N. R. *Adv. Mater.* **2002**, *14*, 80–82. (c) Eustis, S.; El-Sayed, M. A. *Chem. Soc. Rev.* **2006**, *35*, 209–217. (d) Chen, J.; Wiley, B. J.; Xia, Y. *Langmuir* **2007**, *23*, 4120–4129.

(4) (a) PimpinelliA., VillainJ., *Physics of Crystal Growth*, Cambridge University Press: Cambridge, 1998. (b) Xiong, Y.; Xia, Y. *Adv. Mater.* **2007**, *19*, 3385. (c) Xiong, Y.; Cai, H.; Wiley, B. J.; Wang, J.; Kim, M. J.; Xia, Y. *J. Am. Chem. Soc.* **2007**, *129*, 3665–3675.

(5) (a) Kim, J.-U.; Cha, S.-H.; Shin, K.; Jho, J. Y.; Lee, J.-C. *Adv. Mater.* **2004**, *16*, 459–464. (b) Song, J. H.; Kim, K.; Kim, D.; Yang, P. *Chem.−Eur. J.* **2005**, *11*, 910–916.

(6) (a) Sun, X.; Dong, S.; Wang, E. *Langmuir* **2005**, *21*, 4710–4712. (b) Zhang, J.; Gao, Y.; LlvarezPuebla, R. A.; Buriak, J. M.; Fenniri, H. *Adv. Mater.* **2006**, *18*, 3233–3237. (c) Li, C. C.; Cai, W. P.; Cao, B. Q.; Qun, F. Q.; Li, Y.; Kan, C. X.; Zhang, L. D. *Adv. Funct. Mater.* **2006**, *16*, 83–90.

(7) (a) Malikova, N.; Pastoriza-Santos, I.; Schierhorn, M.; Kotov, N. A.; Liz-Marzán, L. M. *Langmuir* **2002**, *18*, 3694–3697. (b) Sau, T. K.; Murphy, C. J. *J. Am. Chem. Soc.* **2004**, *126*, 8648–8649. (c) Murphy, C. J.; Sau, T. K.; Gole, A. M.; Orendorff, C. J.; Gao, J. X.; Gou, L. F.; Hunyadi, S. E.; Li, T. *J. Phys. Chem. B* **2005**, *19*, 13857–13870.

(8) (a) Shankar, S. S.; Rai, A.; Ankamwar, B.; Singh, A.; Ahmad, A.; Sastry, M. *Nat. Mater.* **2004**, *3*, 482–488. (b) Shao, Y.; Jin, Y.; Dong, S. *Chem. Commun.* **2004**, 1104–1105. (c) Shankar, S. S.; Rai, A.; Ahmad, A.; Sastry, M. *Chem. Mater.* **2005**, *17*, 566–572. (d) Xie, J.; Lee, J. Y.; Wang, D. I. C.; Ting, Y. P. *Small* **2007**, *3*, 672–682. (e) Tan, Y. N.; Lee, J. Y.; Wang, D. I. C. *J. Phys. Chem. C* **2008**, *112*, 5463–5470.

10.1021/la802279j CCC: $40.75
Published on Web 10/17/2008

size-controlled Au nanostructures, such as nanowires,[5] rods,[5b,7b,9] nanoplates,[5a,6a,c,7a,8,10] belts,[11] multipods,[7b,12] and nanocrystals of different geometries (cubes,[7b,13] tetrahedra,[14] octahedra,[6b,13b,14,15] decahedra,[16] icosahedra[14,16b,17] and bipyramids[18]) were obtained in high yield in recent years.

Many applications of Au NPs require these particles to be water dispersible and to remain suspended in water with no loss of physical or chemical properties over extended periods of time.[1d,19] Moreover, the utility of these particles in biological applications, however, will require much more than mere water solubility, the stability of these NPs in high ionic strength environments will become very important. Thus, stabilization is an important and challenging task to prevent NPs from aggregation and to finely control their size and shape.[1d,2d] In addition, utilization of nontoxic chemicals, environmentally benign solvents, and renewable materials are emerging issues that merit important consideration in synthetic strategies.[20] In this regard, very recently Sakai et al.[21] reported an environmentally friendly single-step synthesis and stabilization of Au NPs in aqueous solution containing poly(ethylene oxide)-poly(propylene oxide)-poly(ethylene oxide) block copolymer solutions at ambient temperature (known as Pluronics, $E_mP_nE_m$, where E and P denote an ethylene oxide and a propylene oxide unit, respectively, and the subscripts the block lengths), where the block copolymers were proved to be multifunctional macromolecules in the reduction reaction, that is, they were efficient both as reductants and colloidal stabilizers. These copolymers are commercially available, inexpensive, nonionic, high-molecular weight materials that have exciting properties[22] and can be used in different applications such as drug delivery[23] and templates in the synthesis of mesoporous materials.[24] This synthetic method has been successfully applied to obtain Au,[21a,b,26a,b] Ag[21c,d] and Pd[26c] NPs with quasispherical shapes and sizes between ca. 4−30 nm. In the case of palladium salt, solutions at very low pH gave rise to the obtention of dendritic Pd NPs, whereas the addition of different volumes of a growing solution to palladium seeds allowed the formation of polydisperse angled NPs but without a well-defined shape.[26c]

In the present work, we report the production of uniform isotropic (spherical or quiasispherical) and anisotropic (nanoplates) gold nanoparticles in an efficient one-pot aqueous-phase synthesis from the reduction of Au salts by using polyethylene oxide-polystyrene oxide triblock copolymers as both reductants and stabilizers, in which the inner block is an oxyphenylethylene unit (denoted as S, $OCH_2CH(C_6H_5)$). We use these copolymers to put more light on the role of copolymer hydrophobicity and structure on nanoparticles synthesis. This type of block copolymers are denoted as $E_mS_nE_m$ and are commercially available from Goldsmicht AG (Essen, Germany), although those used in the present study were synthesized in laboratory.[27] The effects of enviromentally factors such as temperature and reactants concentrations on particle size and shape were also systematically studied. This single-step synthetic route allows obtaining high yields of metallic nanoparticles with controlled size by changing the solution conditions as made in previously well-established methods such as citrate reduction,[28] (a) the Brust-Schiffrin reaction method,[28] (b) reduction in microemulsions,[28] (c) thermal decomposition,[6b] seeding,[28] (d) photochemistry[28] (e), sonochemistry,[28] (f) radiolysis,[28] (g) and so forth, but solve several problems: the use of organic solvents, byproducts from the reducing agent, the need for an external energy supply such as heating, photo- or ultrasound irradiation, and a high concentration of protective agent required to attain colloidal stability of nanoparticles.[29]

In particular, we have found that the combination of a larger hydrophobicity of the present copolymers, if compared to Pluronic block copolymers,[30] and moderate temperatures results in size-tunable nanoplate formation as a consequence of the very mild reducing power of the block copolymer. This leads to a kinetically controlled synthesis of nanoparticles provided that mainly steps (b) and (c) of the previously mentioned reaction mechanism are largely influence by copolymer hydrophobicity,[21] so preferential adsorption of the block copolymer on certain crystallographic planes can favor the growth on specific nanocrystal facets to

(9) (a) Nikoobakth, B.; El-Sayed, M. A. *Chem. Mater.* **2003**, *15*, 1957–1962. (b) Busbee, B. D.; Obare, S. O.; Murphy, C. J. *Adv. Mater.* **2003**, *15*, 414–416. (c) Pérez-Juste, J.; Pastoriza-Santos, I.; Liz-Marzán, L. M.; Mulvaney, P. *Coord. Chem. Rev.* **2005**, *249*, 1870–1901. (d) Kou, X.; Zhang, S.; Tsung, C.-K.; Yang, Z.; Yeung, M. H.; Stucky, G. D.; Sun, L.; Wang, J.; Yan, C. *Chem.—Eur. J.* **2007**, *13*, 2929–2936.

(10) (a) Ah, C. S.; Yun, Y. J.; Park, H. J.; Kim, W.-J.; Ha, D. H.; Yun, W. S. *Chem. Mater.* **2005**, *17*, 5558–5561. (b) Millstone, J. E.; Park, S.; Shuford, K. L.; Qin, L.; Schatz, G. C.; Mirkin, C. A. *J. Am. Chem. Soc.* **2005**, *127*, 5312–5313. (c) Millstone, J. E.; Métraux, G. S.; Mirkin, C. A. *Adv. Funct. Mater.* **2006**, *16*, 1209–1204. (d) Kan, C.; Zhu, X.; Wang, G. *J. Phys. Chem. B* **2006**, *110*, 4651–4656.

(11) (a) Zhang, J. L.; Du, J. M.; Han, B. X.; Liu, Z. M.; Jiang, T.; Zhang, Z. F. *Angew. Chem., Int. Ed.* **2006**, *45*, 1116–1119. (b) Zhang, Z.; Liu, H.; Wang, Z.; Ming, N. *Adv. Funct. Mater.* **2007**, *17*, 3295–3303.

(12) (a) Chen, S. H.; Wang, Z. L.; Ballato, J.; Foulger, S. H.; Carroll, D. L. *J. Am. Chem. Soc.* **2003**, *125*, 16186–16187. (b) Hao, E.; Bailey, R. C.; Schatz, G. C.; Hupp, J. T.; Li, S. Y. *Nano Lett.* **2004**, *4*, 327–330.

(13) (a) Jin, R. C.; Egusa, S.; Scherer, N. F. *J. Am. Chem. Soc.* **2004**, *126*, 9900–9901. (b) Seo, D.; Yoo, C. I.; Park, J. C.; Park, S. M.; Ryu, S.; Song, H. *Angew. Chem., Int. Ed.* **2008**, *47*, 763–767.

(14) (a) Kim, F.; Connor, S.; Song, H.; Kuykendall, T.; Yang, P. *Angew. Chem., Int. Ed.* **2004**, *43*, 3673–3677.

(15) (a) Seo, D.; Park, J. C.; Song, H. *J. Am. Chem. Soc.* **2006**, *128*, 14863–14870. (b) Li, C.; Shuford, K. L.; Park, Q.-H.; Cai, W.; Li, Y.; Lee, E. J.; Cho, S. O. *Angew. Chem., Int. Ed.* **2007**, *46*, 3264–3268.

(16) (a) Sánchez-Iglesias, A.; Pastoriza-Santos, I.; Pérez-Juste, J.; Rodríguez-González, B.; Abajo, F. J. G.; Liz-Marzán, L. M. *Adv. Mater.* **2006**, *18*, 2529–2534. (b) Liu, X.; Wu, N.; Wunsch, B. H.; Barsotti, R. J., Jr.; Stellacci, F. *Small* **2006**, *2*, 1046–1050.

(17) Xu, J.; Li, S.; Weng, J.; Wang, X.; Zhou, Z.; Yang, K.; Liu, M.; Chen, X.; Cui, Q.; Cao, M.; Zhang, Q. *Adv. Funct. Mater.* **2008**, *18*, 277–284.

(18) Kou, X.; Ni, W.; Tsung, C.-K.; Chan, K.; Lin, H.-Q.; Stucky, G. D.; Wang, J. *Small* **2007**, *3*, 2103–2113.

(19) Fendler, J. H. In *Nanoparticles and Nanostructured Films*; Wiley VCH: Weinheim, 1998.

(20) Raveendran, P.; Fu, J.; Wallen, S. L. *J. Am. Chem. Soc.* **2003**, *125*, 13940–13941.

(21) (a) Sakai, T.; Alexandridis, P. *Langmuir* **2004**, *20*, 8426–8430. (b) Sakai, T.; Alexandridis, P. *J. Phys. Chem. B* **2005**, *109*, 7766–7777. (c) Sakai, T.; Alexandridis, P. *Langmuir* **2005**, *21*, 8019–8025. (d) Sakai, T.; Alexandridis, P. *Nanotechnology* **2005**, *16*, S344−S353.

(22) Hamley I. W. In *The Physics of Block Copolymers*; Oxford Science Publications, 1998.

(23) (a) Rapoport, N. Y.; Herron, J. N.; Pitt, W. G.; Pitina, L. *J. Controlled Release* **1999**, *58*, 153–162. (b) Kabanov, A. V.; Batrakova, E. V.; Alakhov, V. Y. *J. Controlled Release* **2002**, *82*, 189–212. (c) Taboada, P.; Velasquez, G.; Barbosa, S.; Castelletto, V.; Nixon, S. K.; Yang, Z.; Heatley, F.; Hamley, I. W.; Ashford, M.; Mosquera, V.; Attwood, D.; Booth, C. *Langmuir* **2005**, *21*, 5263–5271.

(24) (a) Zhao, D.; Feng, J.; Huo, Q.; Melosh, N.; Fredrickson, G. H.; Chmelka, B. F.; Stucky, G. D. *Science* **1998**, *279*, 548–552. (b) Yang, P.; Zhao, D.; Margolese, D. I.; Chmelka, B. F.; Stucky, G. D. *Chem. Mater.* **1999**, *11*, 2813–2826. (c) Soler-Illia, G. J. A. A.; Crepaldi, E. L.; Grosso, D.; Sanchez, C. *Curr. Opin. Colloid Interface Sci.* **2003**, *8*, 109–126.

(25) Longenberger, L.; Mills, G. *J. Phys. Chem. B* **1995**, *99*, 475–478.

(26) (a) Lai, J. I.; Shafi, K. V. P. M.; Ulman, A.; Loos, K.; Lee, Y.; Vogt, T.; Lee, W.-L.; Ong, N. P. *J. Phys. Chem. B* **2005**, *109*, 15–18. (b) Chen, S.; Guo, C.; Hu, G.-H.; Wang, J.; Ma, J.-H.; Liang, X.-F.; Zheng, L.; Liu, H.-Z. *Langmuir* **2006**, *22*, 9704–9711. (c) Piao, Y.; Jang, Y.; Shokouhimehr, M.; Lee, I. S.; Hyeon, T. *Small* **2007**, *3*, 255–260.

(27) Yang, Z.; Crothers, M.; Ricardo, N. M. P. S.; Chaibundit, C.; Taboada, P.; Mosquera, V.; Kelarakis, A.; Havredaki, V.; Martini, L.; Valder, C.; Collet, J. H.; Attwood, D.; Heatley, F.; Booth, C. *Langmuir* **2003**, *19*, 943–950.

(28) (a) Turkevich, J.; Hillier, J.; Stevenson, P. C. *Discuss. Faraday Soc.* **1951**, *11*, 55–75. (b) Brust, M.; Walker, M.; Bethell, D.; Schiffrin, D. J.; Whyman, R. J. *Chem. Soc., Chem. Commun.* **1994**, 801–802. (c) Pileni, M. P. *Langmuir* **1997**, *13*, 3266–3276. (d) Jana, N. R.; Gearheart, L.; Murphy, C. J. *Chem. Mater.* **2001**, *13*, 2313–2322. (e) Zhou, Y.; Wang, Z. L.; Pal, T. *Chem. Mater.* **1999**, *11*, 2310–2312. (f) Okitsu, K.; Yue, A.; Tanabe, S.; Yobiko, Y. *Langmuir* **2001**, *17*, 7717–7720. (g) Henglein, A.; Meisel, D. *Langmuir* **1998**, *14*, 7392–7396.

(29) Pileni, M. P. In *Fine Particles: Synthesis, Characterization and Mechanism of Growth*; Sugimoto, T., Ed.; Marcel Dekker: New York, 2000; p 497.

(30) Castelletto, V.; Hamley, I. W.; Crothers, M.; Attwood, D.; Yang, Z.; Booth, C. *J. Macromol. Sci. Part B* **2004**, *B43*, 13–27.

Table 1. Molecular Characteristics of the Block Copolymers [a]

	M_n/g mol^{-1} (NMR)	wt% PEO	M_w/M_n (GPC)	M_w/g mol^{-1}	cmc/g l^{-1}
$E_{69}S_8E_{69}$	7030	89	1.05	7380	0.11[a]
$E_{112}S_8E_{112}$	11000	90	1.08	11900	0.14 [a]
$E_{65}S_{11}E_{65}$	7040	81	1.05	7390	0.095[b]
$E_{67}S_{15}E_{67}$	7700	77	1.04	8100	0.025[b]

[a] Estimated uncertainties: M_n to ± 3%; wt% PEO ±1%; M_w/M_n to ±0.01. $M_{w\ calculated}$ from M_n and M_w/M_n.[a] From ITC and [b] from surface tension measurements at 30 °C in ref 24.

give the final shape. Thus, we demonstrate that these block copolymers allow the formation of gold nanoplates by lowering the reduction rate and favoring selective adsorption and surface reduction on {100} planes of metal nuclei. We also verify that the plate sizes can be controlled by varying the copolymer/gold salt molar ratio.

On the other hand, to the best of our knowledge this is the first report on the obtention of gold nanoplates in good yield through a facile aqueous single-step synthesis by using block copolymer as reductants and stabilizers under mild conditions. Previous attempts have been usually based on solution-phase chemical reactions with similar yields to those obtained in the present work but, in general, with a larger size polydispersity and often requiring high temperatures,[10a,d] elaborate procedures as seeded growth,[10b,c] or rare reactants such as proteinic extracts or amino acids.[8] This alternative polymer−water-based system provides a more convenient and environmentally benign route to the synthesis of shape-controlled noble-metal nanocrystals in high yield because it does not involve toxic organic solvents or reagents and serves as a bridge between two frontline discipline: the block copolymer science and crystal nucleation and growth.

2. Experimental Section

Materials. Block copolymers were prepared by sequential anionic polymerization of styrene oxide followed by ethylene oxide (refs 27 and 30 for further details). The molecular characteristics of the copolymers are summarized in Table 1. $HAuCl_4 \cdot 3H_2O$ (99.9% purity) was purchased from Sigma Chemical Co and used without further purification. Water used in all reactions was doubly distilled and degassed before use.

Synthesis of Nanoparticles. Gold nanoparticles were prepared by mixing an aqueous $HAuCl_4$ solution (0.2 mL) of desired concentration with an aqueous block copolymer solution (2 mL) of suitable concentration at a determined temperature. The reported copolymer concentrations throughout the article were those of the aqueous polymer solutions after mixing with the $HAuCl_4$ solution. Solutions were vigorously stirred for 2 min and then kept at suitable temperature in a thermostatted water bath.

The formation of Au NPs by mediated-block copolymer synthesis comprised three main steps:[21] (a) reduction of gold ions by the block copolymer via deoxidation of the E and S segments by the metal center[25] in bulk solution, resulting in the formation of gold clusters;

$$AuCl_4 + lE_nS_mE_n \rightarrow (AuCl_4)-(E_nS_mE_n)_l$$

where $(AuCl_4) - (E_nS_mE_n)_l$ represents $AuCl_4$ ions bound to cavities formed from hydrated E and S coils.

(b) Adsorption of block copolymers on the surface of metal clusters and subsequent reduction of metal ions on the surface of these gold clusters, which involves particle growth.

$$Au_s + lE_nS_mE_n \rightarrow (Au_s)-(E_nS_mE_n)_l$$

where $(Au_s) - (E_nS_mE_n)_l$ represents a gold cluster with adsorbed copolymer, which can form pseudocrown ether structures that bind with $AuCl_4$ ions, $(Au_s) - (E_nS_mE_n)_l - (AuCl_4)$, and facilitated their reduction.

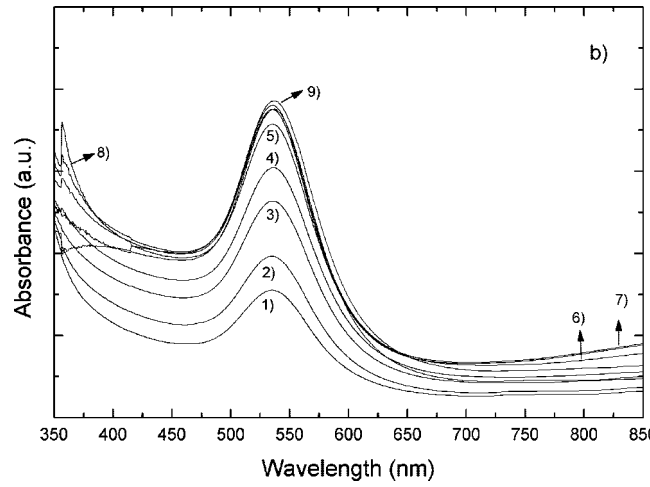

Figure 1. Absorbance spectra of 5 mM $E_{67}S_{15}E_{67}$ block copolymer in the presence of 0.5 mM $HAuCl_4$ at different reaction times: 1) 30 min, 2) 90 min, 3) 6 h, 4) 18 h, 5) 24 h, 6) 48 h, 7) 60 h), 8) 72 h, and 9) 96 h at 25 °C.

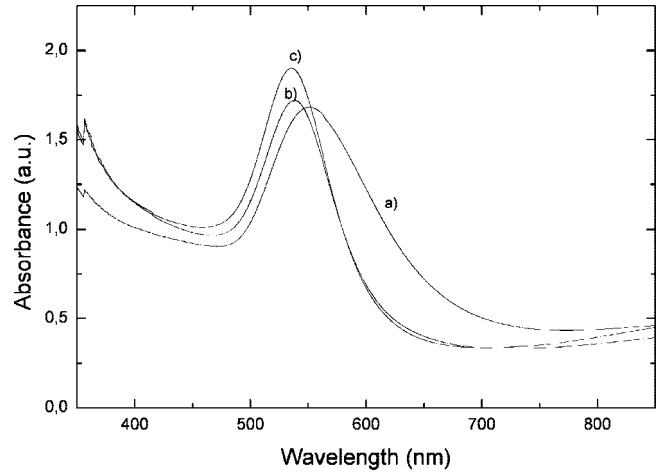

Figure 2. Absorbance spectra in the presence of 0.5 mM $HAuCl_4$ of 5 mM of a) $E_{69}S_8E_{69}$, b) $E_{65}S_{11}E_{65}$, and c) $E_{67}S_{15}E_{67}$ block copolymers at 25 °C.

(c) Final colloidal stabilization of metal nanoparticles by block copolymers.

Characterization of Au NPs. The gold reduction evolution and the optical properties of the prepared NPs were characterized with a Beckman DU series 640 UV−vis spectrometer. To prepare most of TEM and SEM samples, the reacted mixtures were centrifuged once (12 000 rpm for 20 min), the supernatant containing unreduced ions and excess copolymer molecules was removed and the solid redispersed again in water; then, a little drop of the resulting dispersion was simply put onto a carbon-covered copper grid and slowly evaporated on air. Morphologies of the NPs were observed with a transmission electron microscope Phillips CM-12 operated at 120 kV. The size distribution of the gold nanoparticles was obtained by measuring the diameters of more than 200 particles viewed in the micrographs. High-resolution TEM images (HR-TEM) and the electron diffraction patterns (SAED) were obtained by high-resolution electron microscopy (JEM-2010, JEOL Ltd.) in conventional transmission mode operating at 200 kV. SEM micrographs were acquired by using a Leica 440 scanning electron microscope operating at 30 kV. Energy dispersive X-ray microanalysis was made with an Oxford 300 detector connected to the SEM instrument. X-ray diffraction analysis of the samples was carried out using a Siemens D5005 X-ray diffractometer with a rotating anode X-ray generator. Twin Göbel mirrors were used to produce a well-collimated beam of Cu Kα radiation ($\lambda = 1.5418$ Å). Samples were put into capillaries

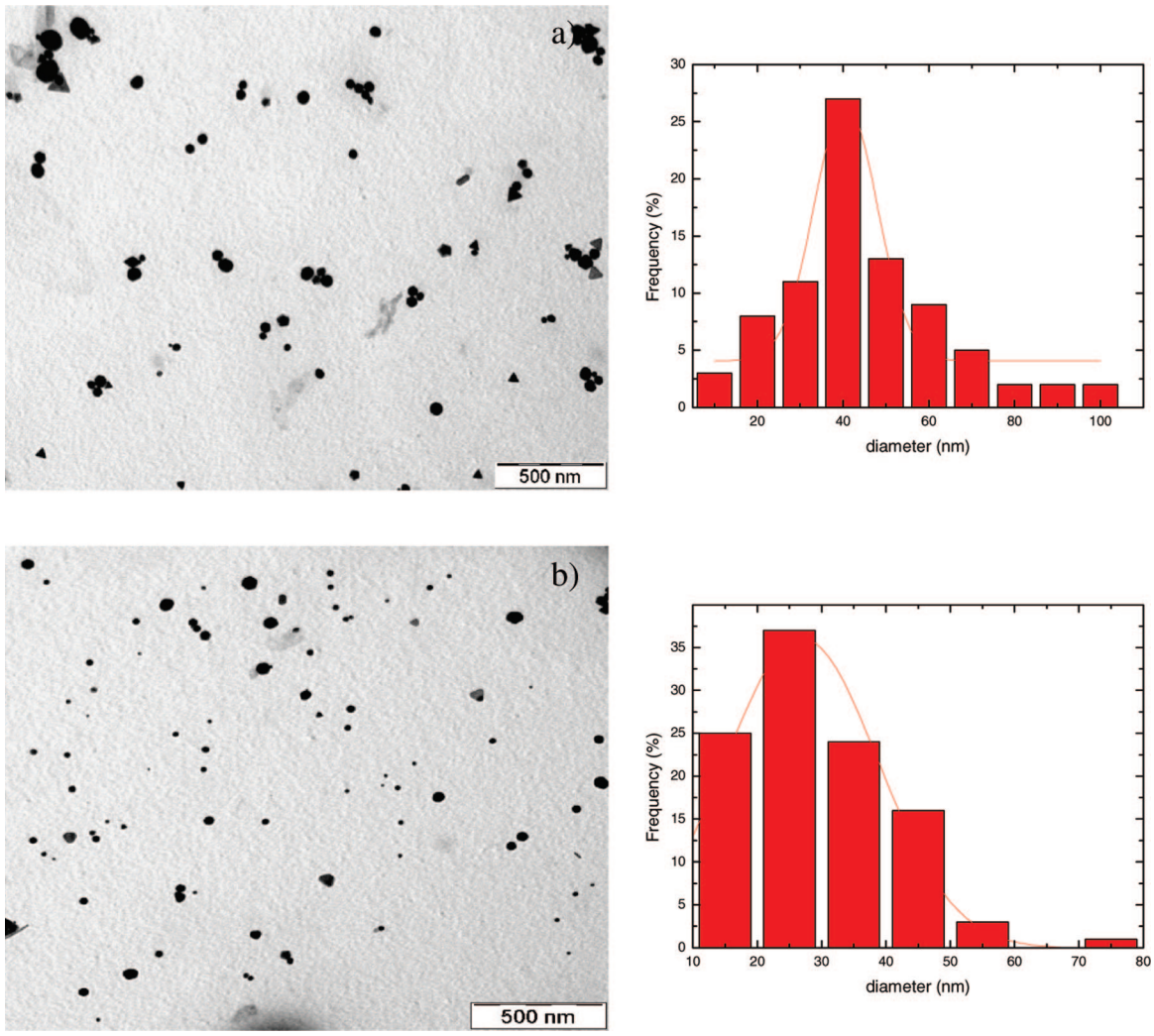

Figure 3. TEM micrographs of gold nanoparticles formed from 0.5 mM $HAuCl_4$ due to reduction in the presence of 5 mM of block copolymers a) $E_{69}S_8E_{69}$ and b) $E_{67}S_{15}E_{67}$ at 25 °C.

with a diameter of 0.5 mm. X-rays diffraction patterns were recorded with an imaging plate detector AXS F.Nr. J2−394. X-ray fluorescence spectroscopy (XRF) was performed in a homemade equipment equipped with a Mo source and a Si−Li semiconductor detector refrigerated in liquid nitrogen.

3. Results and Discussion

Gold nanoparticles were obtained by using three different copolymers, with chemical formulas $E_{69}S_8E_{69}$, $E_{65}S_{11}E_{65}$ and $E_{67}S_{15}E_{67}$. In this way, we could analyze the effect of the copolymer hydrophobic block length on the reduction and stabilization of Au NPs. The self-assembly properties of the three copolymers used in the present study have been previously analyzed by different techniques such as static and dynamic light scattering, surface tension, isothermal titration calorimetry, rheometry, and small-angle X-ray scattering.[27,30]

3.1. Spherical Nnanoparticle Formation by Block Copolymers. The formation of nanoparticles through the reduction of $AuCl_4^-$ ions in block copolymer solutions was examined by following the absorption bands centered at ca. 540 nm originated from the surface plasmon resonance (SPR) of Au NPs.[1d,2a] It was not possible to follow the reaction kinetics by observation of the absoption band centered at ~220 nm corresponding to the gold(III) chloride[31] due to the strong polymer absorption at this wavelength as a result of the presence of phenyl rings in their hydrophobic blocks (Figure SI-1 in the Supporting Information). The necessary reaction time to achieve complete metal salt reduction is larger than that previously reported when using Pluronic block copolymers (2 h),[21] and varies between 6 to 96 h depending on reaction conditions (Figure 1). The delay in reaction completion is related to the larger hydrophobicity of $E_mS_nE_m$ block copolymers: micelles promote polymer entanglements which are known to decrease the ability of forming cavities (pseudocrown ether structures), where $AuCl_4^-$ ions are bound for their reduction via oxidation of the polymer by the metal center,[25] so nucleation becomes a difficult process by the low supersaturation of gold nuclei formed. In addition, polyoxyethylene/polyoxystyrene-based block copolymers are tightly packed in aqueous solution even in the unimer state, giving rise to the so-called unimolecular micelles,[27] and this conformation involves a reduction in the level of hydration of the copolymer chains, which diminishes the contact and subsequent reaction with $AuCl_4^-$ ions.

3.1.1. Effect of Copolymer Hydrophobicity. Figure 2 shows the UV−vis spectra of Au NP formation in the presence of block copolymers $E_{67}S_{15}E_{67}$, $E_{65}S_{11}E_{65}$ and $E_{69}S_8E_{69}$ after reaction completion (Figure SI-2 in the Supporting Information for temporal spectra evolution). The intensity of the ~540 nm SPR band decreases in the order $E_{67}S_{15}E_{67} > E_{65}S_{11}E_{65} > E_{69}S_8E_{69}$ for similar total block copolymer concentrations. This indicates that the S block also contributes to gold reduction provided that the E chain length is fairly similar for all the copolymers. As

(31) Caruso, R. A.; Ashokkumar, M.; Grieser, F. *Langmuir* **2002**, *18*, 7831–7836.

occurred for propylene oxide chains in Pluronic block copolymers, S blocks are also immiscible with metal ions in aqueous solutions, which enhances E block reactivity with metal ions.[32]

On the other hand, the SPR band maximum of Au NPs obtained upon reduction with copolymer $E_{69}S_8E_{69}$ red shifts to ~550 nm, which indicates a slightly larger nanoparticle size.[2a] In addition, the SPR band becomes broader likely because of the larger polydispersity of the resulting nanoparticles as reflected by its larger fwmh value (115 nm, compared to 88 and 71 nm for $E_{65}S_{11}E_{65}$ and $E_{67}S_{15}E_{67}$, respectively). TEM micrographs also confirm this trend (Figure 3). Comparing the different block copolymers, we observe that the average particle diameter when using copolymers $E_{67}S_{15}E_{67}$ and $E_{65}S_{11}E_{65}$ is ca. $35-40 \pm 12$ nm, whereas for $E_{69}S_8E_{69}$ increases up to ca. 55 ± 20 nm. The increase in nanoparticle size for the latter copolymer is consistent with a lower copolymer adsorption onto particle surface: polymer adsorption prevents particle growth and provides particle stabilization, as occurred in other colloidal systems.[28d] The decrease in polymer adsorption for the latter copolymer stems from its lowest hydrophobicity (reflected in its largest cmc value, Table 1) providing a less effective surface coverage of the nanoparticle. In this regard, micellization of block copolymers have been proven to be crucial for the stabilization of gold nanoparticles.[26b] Because the hydrophobic blocks tend to adsorb onto the surface of the primary gold seeds,[33] a larger micelle hydrophobicity is more favorable for the entrapment of gold clusters and, thus, results in a better stabilization of the nanoparticles, in agreement with our results.

The crystalline structure of the resulting nanoparticles was confirmed by recording the X-ray diffraction (XRD) pattern. The XRD pattern (Figure SI-3 of the Supporting Information) of the final products shows sharp peaks corresponding to {111}, {200}, {220}, and {311} diffraction peaks of metallic gold and, thus, indicates that the precipitate is composed of pure crystalline gold.[34] Note that the intensity ratios of the {200} and {220} peaks to the {111} diffraction peak were slightly lower than the bulk value (0.34 and 0.29 versus 0.52 and 0.32), indicating a certain predominance of the (111) facets on the formed nanoparticles. In addition, a chemical analysis of our gold nanoparticles was also carried out by X-ray fluorescence spectroscopy (XRF). The XRF spectrum (Figure SI-4 of the Supporting Information) corresponds perfectly to the electronic transitions giving rise to the L spectrum for gold, which demonstrated that gold nanoparticle formation occurs.[35] On the other hand, the energy dipersion X-ray microanalysis (EDX) also showed (Figure SI-5 of the Supporting Information) one main peak and other low-intensity peaks caused by different-energy level differences of the gold atoms, which reveals that the nanoparticles formed were pure metallic gold. The aluminum peak corresponds to some traces belonging to some uncovered region of the aluminum substrate used for measurements.

3.1.2. Effect of Copolymer Concentration. We have recorded absorption spectra after reaction completion when mixing an $AuCl_4^-$ solution with aqueous $E_{67}S_{15}E_{67}$ solutions of different block copolymer concentrations (part a of Figure 4). We can derive different regimes in nanoparticle formation depending on copolymer concentration:

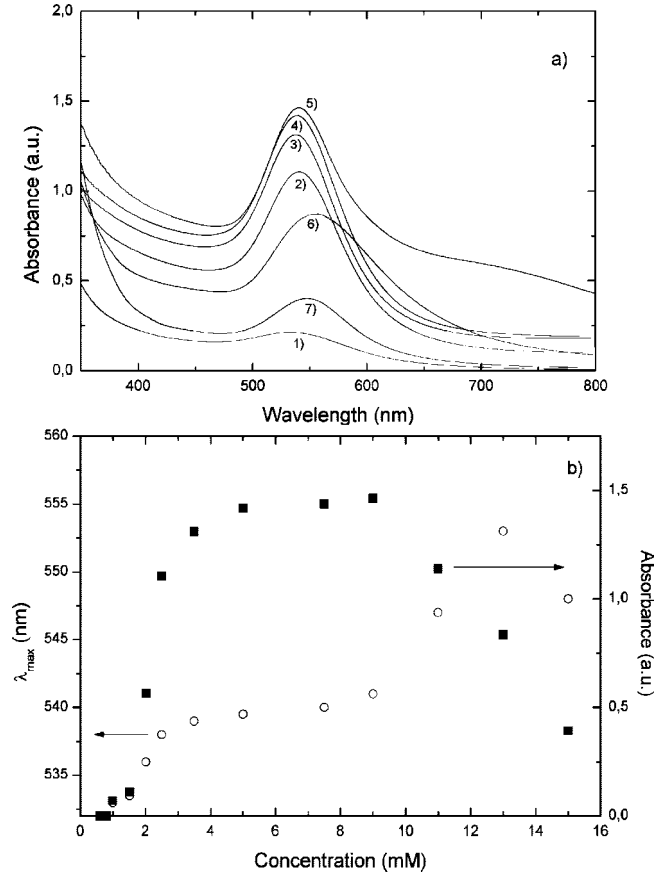

Figure 4. a) Selected absorption spectra of different concentrations of copolymer $E_{67}S_{15}E_{67}$ in the presence of 0.5 mM $HAuCl_4$: 1) 1.5, 2) 2.5, 3) 5, 4) 7.5, 5) 9, 6) 13, and 7) 15 mM at 25 °C. b) Absorption at 540 nm and position of the maximum of the SPR band as a function of copolymer $E_{67}S_{15}E_{67}$ concentration at 25 °C.

a) At copolymer concentrations below 1 mM, nanoparticle formation was almost negligible.

b) Between copolymer concentrations 1.0−9.0 mM, the SPR band at ca. 540 nm becomes progressively more intense and narrower, which points out an increase in the number and monodispersity of the nanoparticles. This behavior is in accordance with the proposed reaction mechanism for nanoparticle formation by Sakai et al.[21b] The wavelength of the SPR maximum also slightly shifts to longer wavelengths (part b of Figure 4), indicating a certain increase in nanoparticle size, as confirmed by TEM graphs (Figure 5). Thus, at 1.5 mM of copolymer the resulting nanoparticles were quite spherical and monodisperse, with number-average diameters of ca. 12 nm; with further copolymer addition (9 mM), the spherical nanoparticles increase their size up to a mean value of ca. 40 nm. In addition, a certain increase in the absorbance at longer wavelengths (600−800 nm) was also observed. This suggests the presence of a certain amount of anisotropic particles (mainly platelet nanoparticles) in solution (part b of Figure 5).[1d] The origin of this increase due to interparticle plasmon coupling originated by particle aggregation is discarded because of the long-term stability of the colloids and because only separate nanoparticles were found by TEM observation.[4a] The formation of various shapes is attributed to an interplay between the faceting tendency of the stabilizing agent and the growth kinetics (rate of supply of Au^0 to the crystallographic planes).[7b]

c) From 9 mM, the absorbance intensity of the SPR band and the subsequent shoulder diminishes, which indicates that the reduction reaction is less effective. Further red-shift of the SPR

(32) Shipway, A. N.; Lahav, M.; Gbai, R.; Willner, I. *Langmuir* **2000**, *16*, 8789–8795.
(33) Cheng, W.; Dong, S.; Wang, E. *Angew. Chem., Int. Ed.* **2003**, *42*, 449–452.
(34) Maye, M. M.; Zheng, W.; Leibowitz, F. L.; Ly, N. K.; Zhong, C.-J. *Langmuir* **2000**, *16*, 490–497.
(35) Wilcoxon, J. P.; Martin, J. E.; Provencio, P. *Langmuir* **2000**, *16*, 9912–9920.

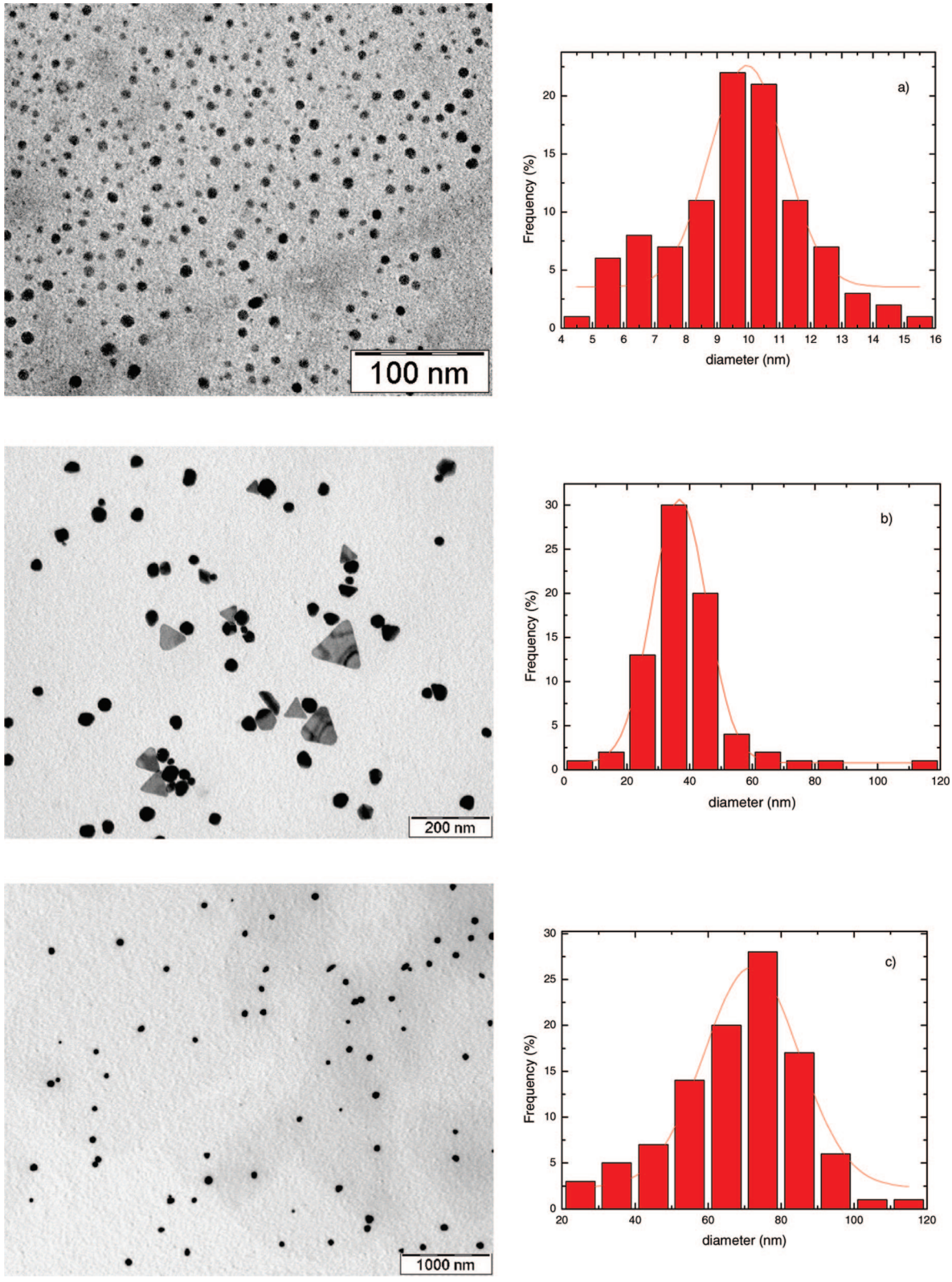

Figure 5. TEM micrographs of gold nanoparticles formed from 0.5 mM $HAuCl_4$ due to reduction in the presence of $E_{67}S_{15}E_{67}$ of concentrations a) 1.5, b) 9, and c) 13 mM at 25 °C.

maximum was observed, in agreement with nanoparticle sizes of ca. 70 nm observed by TEM at a polymer concentration of 13 mM.

In this regard, particle formation and growth are controlled by the amphiphilic (dual-nature) character of the block copolymers: ethylene oxide enhances $AuCl_4^-$ reduction in solution whereas styrene oxide enhances copolymer adsorption on nanoparticle surfaces. This results in a competition between $AuCl_4^-$ reduction in the bulk solution (which leads to an increase in the number of particles) and that on the particle surface (which causes an increase in particle size).[21] In the copolymer concentration range analyzed in the present study, the increase in the number of polymer entanglements in solution (larger number of copolymer micelles) as copolymer concentration increases, seems to

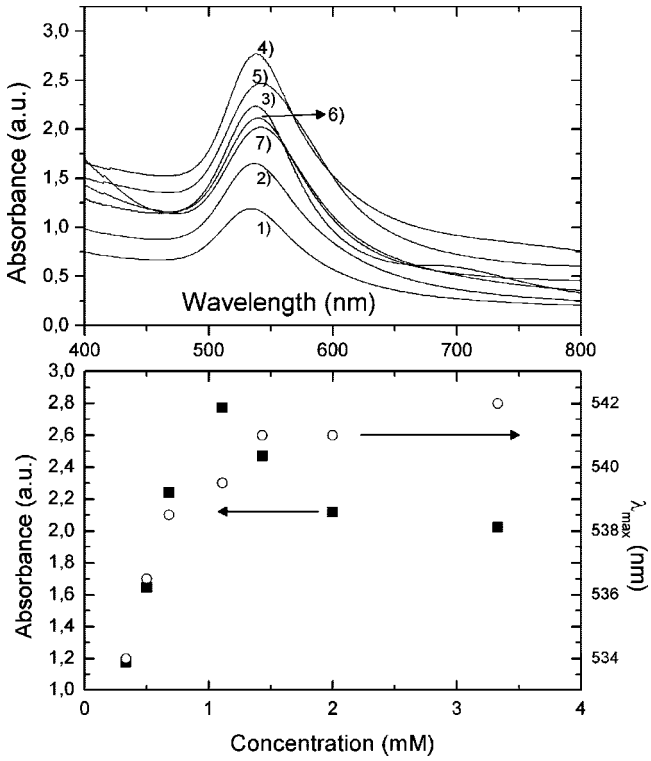

Figure 6. a) Selected absorption spectra of different $HAuCl_4$ salt concentration in the presence of 10 mM $E_{67}S_{15}E_{67}$: 1) 0.3, 2) 0.5, 3) 0.75, 4) 1, 5) 1.5, 6) 2, and 7) 3.5 mM. b) Absorption at 540 nm and position of the maximum of the plasmon surface band as a function of gold salt concentration at 25 °C.

dominate over the larger activity for cavity formation due to the presence of more copolymer molecules in solution: micelles makes less favorable the formation of gold seeds in the nucleation step as a consequence of geometrical constraints and exclude volume effects from one micelle to other, which enables the formation of gold particles with larger sizes.

3.1.3. Effect of Gold Salt Concentration. Part a of Figure 6 shows absorption spectra after reacting different initial $AuCl_4^-$ concentrations (0.3−3.5 mM) with a 10 mM $E_{67}S_{15}E_{67}$ block copolymer solution at 25 °C. As the reaction proceeds, a progressive increase in the absorbance intensity and a blue-shift of the absorption maximum take place (Figure SI-6 of the Supporting Information). The SPR bands of the resulting nanoparticles increase their intensity and slightly red-shift as metal salt concentration increases (part b of Figure 6), which points out a certain increase of the particle size as corroborated by TEM[1]d (Figure SI-7 of the Supporting Information). Quasispherical nanoparticles with diameters ranging between 15−60 nm were observed between 0.3−2.0 mM $AuCl_4^-$; at the highest gold salt concentration (3.5 mM), certain aggregation of Au NPs occurs because of the lack of sufficient block copolymer molecules to correctly stabilize the nanoparticles. In fact, after several weeks of storage, a metal precipitate could be observed.

3.2. Nanoplate Formation by Block Copolymers. Previous studies have shown that one-pot metal nanoparticle synthesis in solution by amphiphilic block copolymers resulted only in the formation of well-stabilized spherical or quasispherical particles.[21,26b,c] Faceted nanoparticles were obtained by adding a growing solution to previously formed spherical seeds[26c] or by using thermal or photoinduced reduction.[5a,6b] We have noted that temperature induces significant changes in the reduction reaction: a) a certain decrease in the reaction rate, b) a variation in the size and shape of the nanoparticles, and c) changes in the reaction yields, provided that polystyrene oxide−polyethylene oxide-based block copolymers display a sensible different temperature-dependent aggregation behavior.[27,28d] This is in contrast with observation made for Pluronic copolymers for which temperature involves an increase in nanoparticle size without appreciable effects on the nanoparticle shape.[21c,27]

In particular, gold nanoplates were synthesized simply by mixing aqueous solutions of $HAuCl_4$ metal salt and block copolymer for 24 h at 65 °C. Upon reaction, the color of the solution changes from light yellow to pink and then, to tint blue, thereby indicating the formation of gold nanoplates.

Figure 7 shows transmission electron microscopy (TEM) images of Au nanoplates synthesized at a copolymer $E_{112}S_8E_{112}$/$HAuCl_4$ molar ratio of 20 at 65 °C. The sample contains approximately 70% moderately sharp plates with lateral size ranging between 150−250 nm without the necessity of separation processes (Experimental Section for further details). To the best of our knowledge, this is the first report on the synthesis of gold nanoplates as a majority product. The absorbance spectrum (part b of Figure 7) is characterized by an absorption band at ∼1050 nm corresponding to the in-plane resonance of the triangular planar objects. Nevertheless, this peak is very sensitive to snipping, and provided that part of our plates do not show acute edges, the absorption maximum is blue-shifted if compared to that of a perfect sharp plate of equivalent size.[10c,d] The broadband at ∼800 nm should correspond to the in-plane quadrupole mode of the nanoplates based on the prediction of the discrete dipole approximation,[10c,d] whereas the band at ∼540 nm relates to the out-of-plane quadrupole resonance of the nanoplates in combination with the plasmon band of some spherical nanoparticles remaining in solution.

Analysis of the nanoplates by selected-area diffraction (SAED) by directing the electron beam perpendicular to the triangular flat faces reveals a regular, hexagonal, diffraction spot array that corresponds to a (111) zone-axis single crystal with an atomically flat surface (part c of Figure 7). Besides the Bragg diffractions spots of {220} and {422} (lattice spacings of 1.4 and 0.8 Å, respectively), the pattern also displays inner 1/3{422} type faint spots (lattice spacing 2.4 Å), which are forbidden in a typical fcc single-crystal structure and are often associated with thin structures enclosed by atomically flat top and bottom facets bound by {111} planes.[8c,d,10a] Their presence has been assigned to the existence of unique (111) stacking faults parallel to the (111) surface extending across the entire particle,[8b,c] to the presence of parallel twin planes, to surface reconstruction, or the combination of twin planes and (111) stacking faults.[36] The XRD recorded from the same sample shows that the intensity ratios of the (200) and (220) peaks to the (111) peak were much lower than the bulk value (0.14 and 0.12 versus 0.52 and 0.32), indicating that nanoplates were dominated by {111} facets (Figure SI-8 of the Supporting Information). The flat nature of nanoplates can be demonstrated by the low contrast observed for the polygonal particles (parts b and c of Figure 7) and by the presence of Moiré patterns arising from the presence of two superimposed, different crystalline lattices can be identified (part d of Figure 7).[37] The thickness of the nanoplates was of ca. 22 ± 5 nm as derived from SEM, demonstrating their flat nature; this does not vary when lateral dimensions change, and nanoplate surface also appears smooth (Figure SI-9 of the Supporting Informationas an example).

(36) (a) Lofton, C.; Sigmund, W. *Adv. Funct. Mater.* **2005**, *15*, 1197–1208. (b) Germain, V.; Li, J.; Ingert, D.; Wang, Z. L.; Pileni, M. P. *J. Phys. Chem. B* **2003**, *107*, 8717–8720. (c) Elechiguerra, J. L.; Reyes-Gasga, J.; Yacaman, M. J. *J. Mater. Chem.* **2006**, *16*, 3906–3919.

(37) Williams, D. B.; Carter, C. B. In *Transmission Electron Microscopy, A Text for Materials Science*; Plenum Press: New York, 1996.

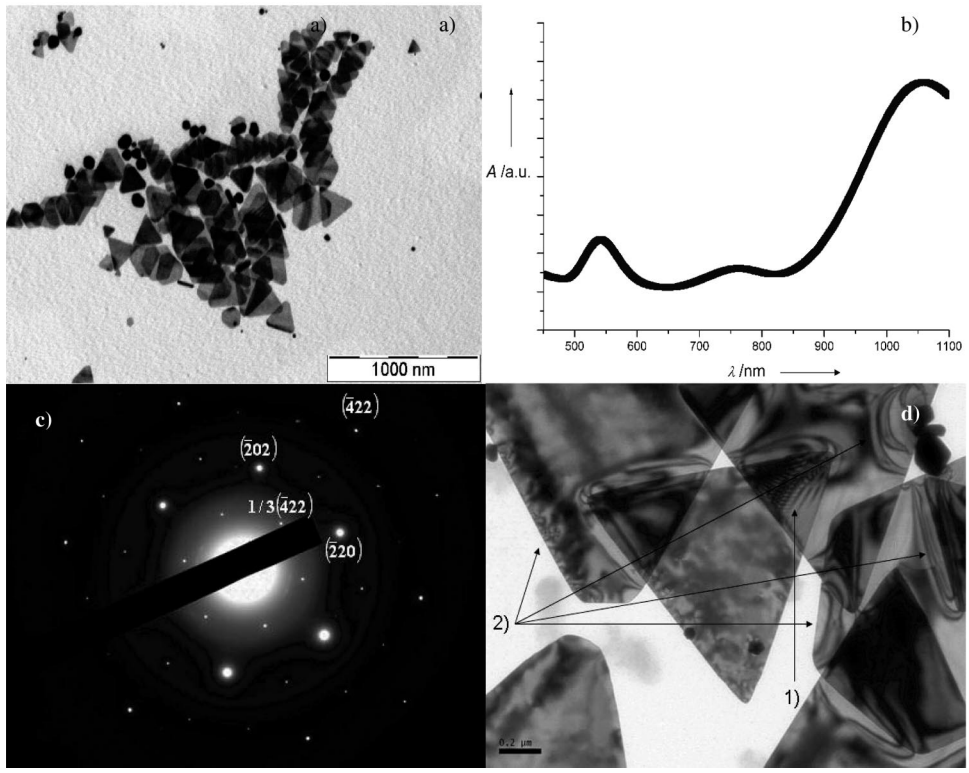

Figure 7. a) TEM graph of Au nanoplates formed at a copolymer $E_{112}S_8E_{112}$/Au salt molar ratio of 20 (0.5 mM $HAuCl_4$) at 65 °C. b) UV−vis spectrum corresponding to such nanoplates. c) SAED pattern taken from an individual nanoplate and its assigned reflection indexes. d) Triangular nanoprims after aging for 1 week with Moiré patterns (1) and bending contours (2).

The plates are also decorated with different bending contours, with diffraction effects resulting from slight bending of thin nanoplates as a consequence of some structural instability of these nanoobjects.[10a]

The reaction temperature was found to be critical for nanoplate formation (Figure SI-10 of the Supporting Information). Carrying out the gold reduction at room temperature resulted in the formation of relatively monodisperse spherical nanoparticles with mean sizes of 70 ± 20 nm, in agreement with a moderately fast reaction. In comparison, at higher temperatures (between 30−65 °C) an increasingly nanoplate population develops as temperature rises, with a maximum at 65 °C (70% yield). At higher temperatures (70 °C and above), the reduction is slow and only irregular and polydisperse particles are present.

Compared to the thermodynamic favored shapes (cuboocta-hedra and multiply twinned particles), the surface energy of nanoplates is much higher so that their formation requires kinetic control. Thus, the mild reducing power of the block copolymer as temperature rises involves that both nucleation and growth turned into kinetic control. As particle formation and growth are controlled by the amphiphilic character of the block copolymers, the decrease in the reaction rate with temperature is a consequence of: a) the presence of very hydrophobic styrene oxide units as the hydrophobic block if compared to other polyethylene oxide/ based block copolymers previously used in nanoparticle synthesis,[21] b) the dehydration of polyoxyethylene chains as temperature rises, and c) selective copolymer adsorption on certain crystallographic planes of the nanocrystals. The two first effects do not facilitate the cavity formation for metal nuclei reduction in solution provided that copolymer micellization is enhanced, favoring chain entanglement and a size increase.

Then, if the reaction rate is slow enough, block copolymer adsorption onto metal clusters/nanoparticles and subsequent surface reduction on that vicinity should become the dominant process:[21b] the rate of creation of new metal nuclei in solution decreases and selective copolymer adsorption on {111} planes of the nanocrystals due to their lowest energy occurs inhibiting the growth on such crystallographic planes, which promotes anisotropic growth along {100} orientation and the formation of (111) bounded structures as thin nanoplates.[2a,8e,10d] At room temperature, the reaction is faster and copolymer chains can accumulate on different crystallographic planes homogenizing the surface structure and disabling the differential growth in different crystallographic directions, so spherical nanoparticles are formed. On the other hand, we cannot disregard the role of the etchant O_2/Cl^- pair to eliminate twinned particles and favor nanoplate formation, whose effectiveness increases as temperature raises.[4] In fact, if the reaction is made under inert argon atmosphere at 65 °C, the nanoplate yield decreases by 20%.

Nanoplates in good yields were also obtained when using other polystyrene oxide−polyethyelene oxide block copolymers in the reaction. In particular, reactions in the presence of 5 mM of copolymers $E_{69}S_8E_{69}$ and $E_{67}S_{15}E_{67}$ at 65 °C result in triangular nanoplates with lateral mean sizes of 170 ± 50 and 210 ± 40 nm. Also a significant population of hexagonal plates with lateral size of 132 ± 18 nm was obtained with the latter copolymer (Figure SI-11 of the Supporting Information). The presence of this type of shape is indicative of a decrease in the reaction rate provided that low reaction rates difficult the evolvement from hexagonal to triangular forms.[38] On the other hand, the increase in nanoplate lateral size in the presence of the former copolymers can be explained by the longer ethylene oxide blocks of copolymer $E_{112}S_8E_{112}$.

3.2.1. Growth Mechanism. To elucidate the growth mechanism of the gold nanoplates, we monitored the evolution of their shape

(38) (a) Washio, I.; Xiong, Y.; Yin, Y.; Xia, Y. *Adv. Mater.* **2006**, *18*, 1745–1749. (b) Xiong, Y.; Washio, I.; Chen, J.; Cai, H.; Li, Z.-Y.; Xia, Y. *Langmuir* **2006**, *22*, 8563–8570.

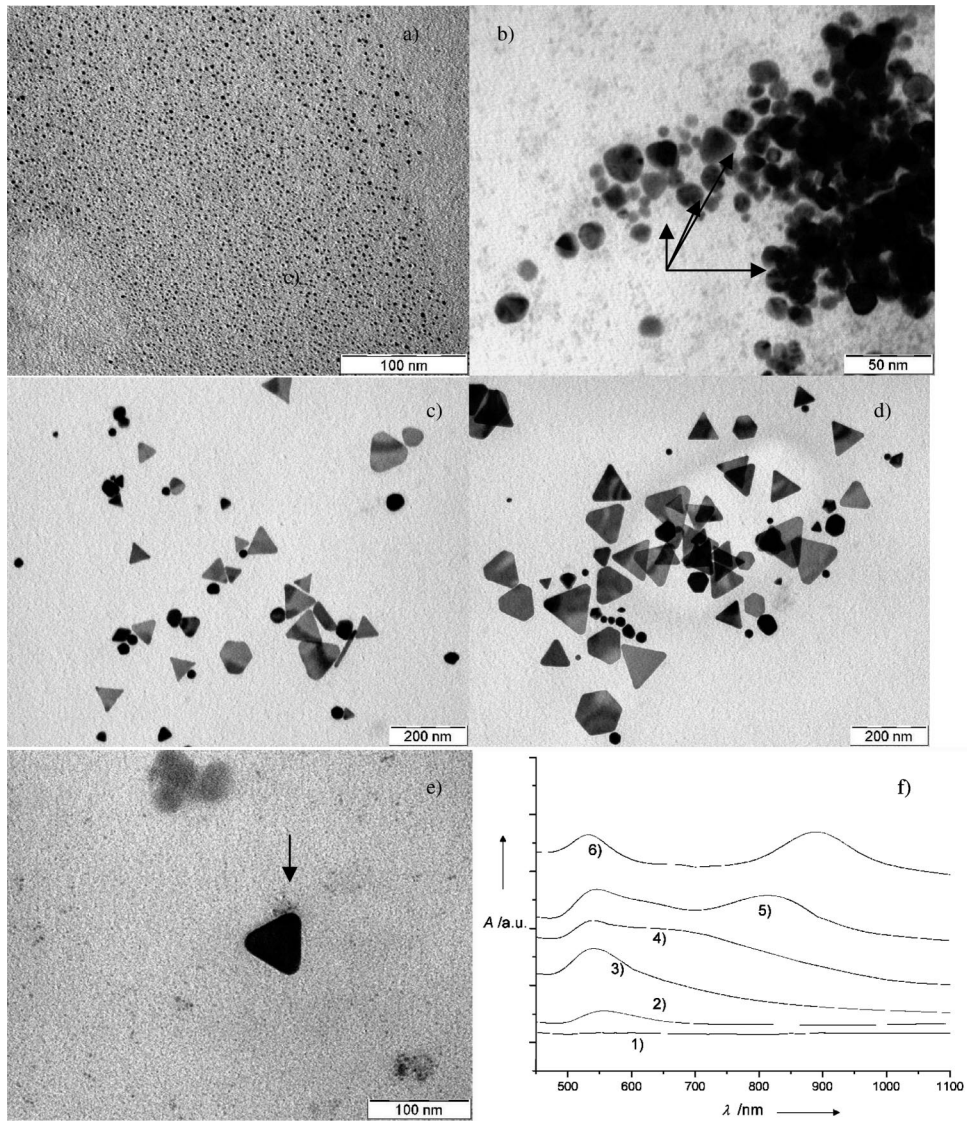

Figure 8. TEM pictures of gold nanoplates formed at a copolymer $E_{112}S_8E_{112}$/Au salt molar ratio of 10 (0.5 mM $HAuCl_4$) at 65 °C at a) 0.5, b) 3, c) 8, and d) 24 h after starting the reaction. Arrows in b) shows the existence of small triangular seeds; e) Typical triangular gold nanoparticle with corrugated structure. The arrow indicates the attachment of gold clusters on the active growth site of the triangular particle. f) UV−vis spectra as a function of time of gold nanoplate reaction: curves 1−7 correspond to spectra recorded at 0, 0.5, 3, 8, 14, and 24 h respectively after starting the reaction.

with TEM by taking samples at various reaction times. Parts b and c of Figure 8 show TEM images of Au NPs were sampled at 0.5, 3, 10, and 24 h, respectively. At $t = 0.5$ h, the sample contains tiny gold seeds with sizes less than 5−7 nm, which can be single or twinned nanocrystals, and display a weak absorption peak centered at ca. 550 nm (spectrum 2, part f of Figure 8). At $t = 3$ h, small triangular gold seeds with sizes between 10−15 nm starts to be observed (part b of Figure 8, see arrows), although quasispherical ones are predominant, which could be either cubooctahedral or multi-twinned particles (MTPs). We cannot distinguish if these particles are planar or not, although the low contrast of some of them might indicates planarity. Some other authors have also reported the formation of triangular seeds of similar dimension than those of the present work in the early stages of their reactions.[1c,8d] Simultaneously, a certain broadening of the surface plasmon band also occurs (spectrum 3, part f of Figure 8), with a shoulder around 650 nm. At $t = 10$ h, nanoplates starts to become the main product (part c of Figure 8), with lateral sizes between 30−80 nm, corresponding well with the appearance of a new SPR signal at 700−800 nm from the in-plane dipole resonance of gold nanoplates (spectra 4 and 5, part f of Figure 8). After 24 h, nanoplates with relatively sharp edges grew to their final sizes of ca. 100 nm, with a further red-shift of the SPR band (spectra 6, part f of Figure 8). Most of the small nanocrystals below a certain size have disappeared, whereas the larger nanoplates have become bigger, thereby suggesting the involvement of Ostwald ripening in the growth process. This growth seems to occur by attachment of gold seeds on the active growth sites of the nanoplates following the most energetically favored direction (part e of Figure 8).

Therefore, the possible growth process might be reconstructed from these TEM images and UV−vis spectra and would include the following steps: a) reduction of Au^{III} ions to form gold nuclei, b) formation of quasispherical, planar and triangular seeds, c) growth of these seeds to nanoplates, and d) further lateral size increase by aging and/or Ostwald ripening (Scheme 1).

3.2.2. Size Control of the Nanoplates. The nanoplate size could be adjusted conveniently by changing the copolymer/gold salt ratio. Figure 9 shows TEM images and UV−vis spectra of gold nanoplates obtained at different copolymer concentrations. Table 2 provides a summary of reaction yields and size distributions of the products. The copolymer/gold salt molar ratio was found

Scheme 1. Representation of the Growth Process of Gold Nanoplates

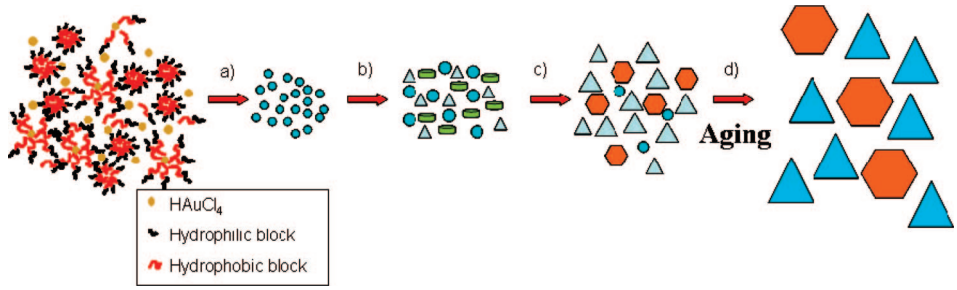

to influence both the size and shape of the gold nanoplates: An increase in the copolymer concentration led to an increase in the lateral average size of the plates from ca. 0.1 up to ca. 0.6 μm after reaction completion. This increase involves a progressive red shift of the in-plane dipole resonance. In fact, maxima in spectra 3 and 4 of part d of Figure 9 lied out of the range of the instrument used. The growth is a consequence of an increase in the number of polymer entanglements in solution (larger number of copolymer micelles) as copolymer concentration increases, as mentioned before. We also observed that aging of the nanoplates in the original solution (1 week) can further extend the lateral size increase their mean size up to $\sim$1.0 μm. Such growth is attributed to the combination of residual reduced Au^0 atoms and gold clusters in solution and an Ostwald ripening process which involves the disappearance of the smaller triangular plates.

4. Conclusions

In summary, isotropic and anisotropic gold nanoparticles in good yield have been obtained by using amphiphilic polyethylene oxide−polystyrene oxide block copolymers in a one-pot synthetic route as both reductant and stabilizer agents in water solutions. Spherical or quasispherical nanoparticles were obtained at room temperature, with their mean size and polydispersity depending on solution conditions, that is, on copolymer block length, copolymer concentration and gold salt concentration. In this regard, an increase in copolymer hydrophobic block length (and, therefore, copolymer hydrophobicity) reduces nanoparticle polydispersity and improves particle stability. This points out that the hydrophobic block plays a much more important role in this type of nanoparticle formation than previously described for other copolymers. Nanoparticle sizes increased as the copolymer concentration increased. An increase in nanoparticle number and size is also observed when a larger amount of gold salt is added to solution. On the other hand, gold nanoplates have been also obtained, whose size and shape can be easily modified by adjusting the reaction temperature and the copolymer/gold salt ratio. This safe purely copolymer-based system enables a facile and green synthetic route to the obtention of nanoplates with tunable absorption in the near-infrared region, which makes them very

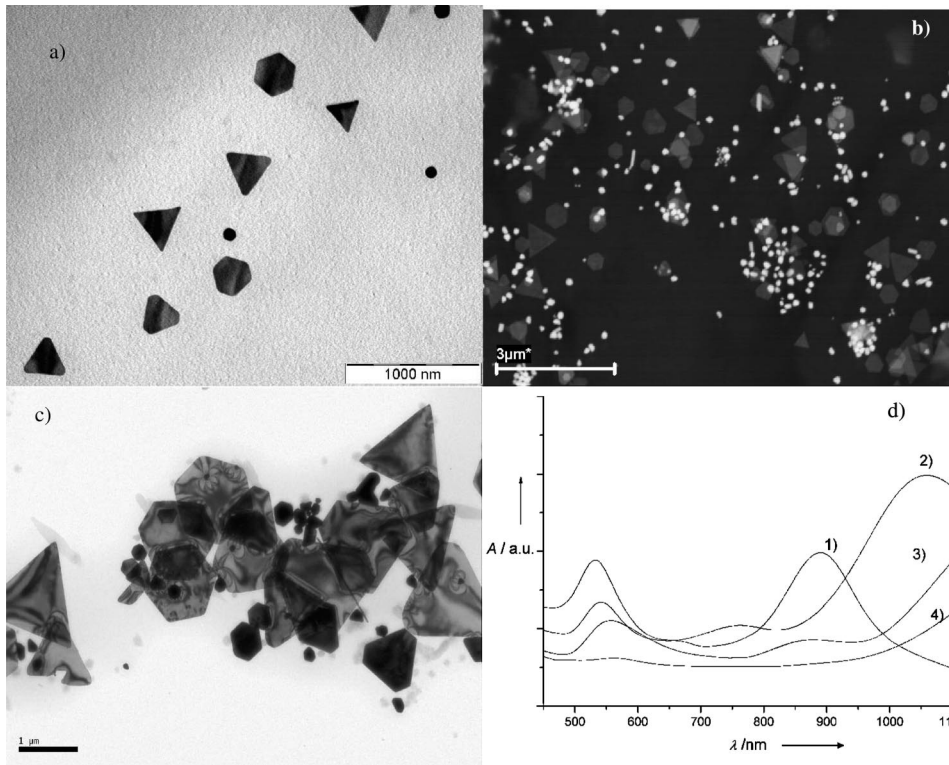

Figure 9. TEM and SEM pictures of gold nanoplates formed by reaction of copolymer $E_{112}S_8E_{112}$/Au salt ratio of a) 30, b) 40, and c) 40 after 1 week of aging at 65 °C. In part b (SEM), bright particles are quasispherical nanoparticles, whereas the plates appear in gray. d) UV−vis spectra of gold nanoplates of different lateral sizes at $E_{112}S_8E_{112}$/gold salt molar ratios of 1) 10, 2) 20, 3) 30, and 4) 40.

Table 2. Summary of the Yield and Lateral Size of the Gold Nanoplates Obtained under Different Experimental Conditions (0.5 mM $HAuCl_4$)

polymer/gold molar ratio	T/°C	product morphology (nanoplate size/nm)
$E_{112}S_8E_{112}$		
20	25	spherical particles (∼98%, 70 ± 20)
20	40	spherical particles (∼90%, 85 ± 35)
20	50	triangular plates (∼30%, 110 ± 55)
20	65	triangular plates (∼70%, 205 ± 35)
20	75	irregular particles (∼85%, 45 ± 40)
20	85	irregular particles (∼95%, 13 ± 15) triangular plates (∼60%,
10	65	105 ± 45)
30	65	triangular and hexagonal plates (∼65%, 370 ± 125)
40	65	triangular and hexagonal plates (∼50%, 575 ± 180)
40	65 (1 week aging)	triangular and hexagonal plates (∼70%, 970 ± 570)
$E_{69}S_8E_{69}$		
10	65	triangular plates (∼65%, 170 ± 50)
$E_{67}S_{15}E_{67}$		
10	65	triangular and hexagonal plates plates (∼55%, 210 ± 40)

interesting in applications such as optical coatings, SERS, and cancer cell hyperthermia.

Acknowledgment. Authors thank Ministerio de Educación y Ciencia by project MAT-2007-61604. E. C. thanks MEC for his postdoctoral fellowhip.

Supporting Information Available: Absorbance spectra, XRD patterns, X-ray fluoresence spectra, TEM micrographs, and SEM pictures of compounds in this article. This material is available free of charge via the Internet at http://pubs.acs.org.

LA802279J